IV.G.1 Clean Energy Research*

Dr. Ralph E. White (Primary Contact),
Dr. John Weidner, Dr. James Ritter,
Dr. Michael Matthews, Dr. John Van Zee,
Dr. Jerome Delhommelle
University of South Carolina
College of Engineering and Information Technology
Columbia, SC 29208
Phone: (803) 777-3270; Fax: (803) 777-6769
E-mail: white@engr.sc.edu

DOE Technology Development Manager:
Carole Read
Phone: (202) 586-3152; Fax: (202) 586-9811
E-mail: Carole.Read@ee.doe.gov

DOE Project Officer: Paul Bakke
Phone: (303) 275-4916; Fax: (303) 275-4753
E-mail: Paul.Bakke@go.doe.gov

Contract Number: DE-FC36-04GO14232

Subcontractors:
Savannah River National Laboratory, Aiken, SC
South Carolina State University, Orangeburg, SC

Start Date: June 1, 2004
Projected End Date: May 31, 2007

*Congressionally directed project

Objectives

- Advancing thermochemical hydrogen production processes.
- Studying the effect of metal dopants, carbon additive, and Al powder on the dehydrogenation and hydrogenation kinetics of complex metal hydrides (e.g. alanates) for on-board hydrogen storage.
- Investigating the gravimetric efficiency and kinetics of steam hydrolysis of sodium borohydride for on-board hydrogen storage and hydrogen production.
- Analyzing the effect of CO, NH_3, and H_2S on fuel cell membrane electrode assembly durability.
- Developing mathematical models to characterize the performance and aging of fuel cell cathodes.
- Molecular simulation of hydrogen storage materials.

Technical Barriers

This project addresses the following technical barriers from the Hydrogen, Fuel Cells and Infrastructure Technologies Program Multi-Year Research, Development and Demonstration Plan:

- Objective #1 addresses technical barriers associated the cost of hydrogen production.
- Objective #2 addresses System Cost (B), System Weight and Volume (A), Durability/Operability (D), and Lack of Understanding of Hydrogen Physisorption and Chemisorption (P) barriers for the development of a viable on-board hydrogen storage system.
- Objective #3 addresses the on-board hydrogen storage technical barriers for System Weight and Volume (A) and Thermal Management (J).
- Objective #4 addresses Durability (A) for fuel cells.
- Objective #5 addresses the Durability (A) and Cost (B) barriers associated with fuel cells.
- Objective #6 identifies suitable materials for hydrogen storage using molecular simulations.

Technical Targets

- Objective #1 – These studies will be applied toward meeting the cost target for production of hydrogen from high-temperature thermochemical cycles of $3/gge.
- Objectives #2 and #3 – Insights gained from these studies will be applied toward the design and synthesis of hydrogen storage materials that meet the following DOE 2010 hydrogen storage targets:
  - Cost: $4/kWh net
  - Specific energy: 2 kWh/kg
  - Energy density: 1.5 kWh/L
- Objectives #4 and #5 – Insights gained from these studies will be applied towards the design and synthesis of the polymer electrolyte membrane (PEM) fuel cell that meets the following DOE 2010 targets listed in Table 3.4.4 of the Multi-Year Research, Development and Demonstration Plan:
  - Cost: $30/kW
  - Durability: 5,000 hours.
- Objective #6 – Molecular Simulations of Hydrogen Storage Materials

Accomplishments

Objective #1 – Low Temperature Electrolytic Hydrogen Production

- Built a PEM electrolyzer to convert HBr to Br_2 and H_2. Achieved 20 kA/cm^2 at cell voltages lower

than 2 V for HBr to Br_2 and H_2. This is a 10-time improvement in performance over previous attempts.
- Generated hydrogen from a PEM electrolyzer by feeding it gaseous HBr.
- Built a PEM electrolyzer to convert SO_2 to H_2SO_4 and H_2.
- Generated hydrogen from a PEM electrolyzer by feeding it gaseous SO_2. Achieved 10 kA/m^2 at cell voltages lower than 1 V SO_2 to H_2SO_4 and H_2. This is a 2.5-time improvement in performance over previous attempts (*i.e.,* Westinghouse process). This improved performance was achieved at one-tenth the Pt loading.
- Developed a preliminary mathematical model to predict electrolyzer performance.

Objective #2 – Development of Complex Metal Hydride Hydrogen Storage Materials

- Discovered a synergistic effect of co-dopants on the dehydrogenation kinetics of sodium aluminum hydride.
- Revealed the effect of graphite on the dehydrogenation and hydrogenation kinetics of ti-doped sodium aluminum hydride.
- Developed a sonochemical doping technique for Ti-catalyzed sodium aluminum hydride.
- Studied the kinetic behavior of Ti-doped sodium aluminum hydride when co-catalyzed with carbon nanostructures.
- Developed a physiochemical pathway for cyclic dehydrogenation and rehydrogenation of $LiAlH_4$.

Objective #3 – Hydrogen Storage Using Chemical Hydrides

- The primary experimental apparatus has been rebuilt to improve the performance of the system.
- A prototype hydrogen generation reactor has been developed. Proprietary details have been disclosed to the University of South Carolina Research Foundation.
- Yields of hydrogen were improved by about 4% with the use of acetic acid, but the use of methanol was ineffective for the improvement of the yield.
- Characterization of the solid product of the hydrolysis reaction by use of thermal gravimetric analysis (TGA), differential scanning calorimetry (DSC), x-ray diffraction (XRD) and ^{11}B NMR indicated that $NaBO_2 \cdot 2H_2O$ is the main byproduct. The ^{11}B nuclear magnetic resonance (NMR) data indicated that the conversion of $NaBH_4$ to $NaBO_2$ is consistent with the measured H_2 yields.
- Heats of formation have been calculated for sodium metaborate for different degrees of hydration ($NaBO_2 \cdot x\ H_2O$).
- An NSF SBIR subcontract will be awarded through Millennium Cell, Inc.

Objective #4 – Diagnostic Tools for Understanding Chemical Stresses and MEA Durability Resulting from Hydrogen Impurities

- Experiments completed to understand the effect of ionomer wt% in the catalysts layer on the rates of NH_3 poisoning of anode. A kinetic analysis suggests that the reaction of NH_3 with the ionomer sites obeys a pseudo-first order reaction with a reaction rate constant of $k=1.2\ h^{-1}$.
- Methodology developed for 3-D predictions of degrading effects. Analysis of similarities and differences in concentration and dosage effects between data for CO for NH_3 and H_2S completed. Model equations for NH_3 and H_2S formulated.
- The degradation with NH_3 does not follow the same mechanism of competitive adsorption that is apparent with CO in H_2 mixtures.

Objective #5 – Developing mathematical models to characterize the performance and aging of fuel cell cathodes

- Confirmed the literature finding that the oxygen reduction reaction (ORR) exhibits a change in Tafel slope, e.g., at high cathode potential, the ORR exhibits a normal Tafel slope and at low cathode potential, a double Tafel slope.
- Demonstrated the need to include in the modeling of a PEM fuel cell a kinetic equation which has the ability to predict such Tafel slope change with cathode potential.
- Collected reliable rotating disk electrode (RDE) data over a wide range of temperatures, e.g., from 30 to 70ºC, and over a wide range of rotating speeds, e.g, from 400 to 3,600 revolutions per minute (rpm).
- An oxygen adsorption model is developed and studied. Simulation and regression based on this model were made on the polarization curves of ORR in 0.5M H_2SO_4 solution at an RDE. The results verified that this model can predict the double Tafel slope phenomena and can fit experimental data better than the normal four electrode mechanism, model does.

Objective # 6 – Molecular Simulation of Hydrogen Storage Materials

- Modelling Hydrogen Storage in Clathrate Hydrates
- Modelling Hydrogen Storage in Metal-Organic Frameworks.
- Modelling Hydrogen Storage in Doped Single and Multi-Metal hydrides.

Objective #1 – Low Temperature Electrolytic Hydrogen Production (Dr. John Weidner)

Introduction

Thermochemical cycles produce hydrogen through a series of chemical reactions that result in the splitting of water at much lower temperatures (~800-1,000ºC) than direct thermal dissociation (>2,500ºC) [1,2]. All other chemical species in these reactions are recycled resulting in the consumption of only heat and water to produce hydrogen and oxygen. Since water rather than hydrocarbons are used as the source of hydrogen, no carbon dioxide emissions are produced and the hydrogen produced is highly pure.

Although there are hundreds of possible thermochemical cycles that can produce hydrogen from water, the two leading candidates are the sulfur-based cycles and the calcium-bromide-based cycles [3-5]. The sulfur-based processes all have the common oxygen generating, high-temperature step, which is the decomposition of sulfuric acid to sulfur dioxide and oxygen at temperatures in the 850-1,000ºC range. In the sulfur-iodine (S-I) cycle, the SO_2 is converted back to H_2SO_4 and hydrogen is produced via a two-step process involving iodine. The distillation of hydrogen iodide (HI) from solution and concurrent decomposition to iodine is the most difficult process issue for the iodine containing portion of the cycle [4,5].

In the 1970s, Westinghouse Electric Corporation developed the hybrid sulfur process, which eliminated the use of iodine completely [6,7]. They electrochemically oxidized SO_2 to H_2SO_4 from a liquid-phase anode stream. Westinghouse demonstrated this process on a scale of 150 l/h of hydrogen in 1976, and a conceptual plant design has been developed.

The calcium-bromide-based cycles also have the potential of high efficiencies but with lower temperature requirements than the sulfur-based cycles (~750ºC). The common step in these cycles is the conversion of CaO and Br_2 to $CaBr_2$ and O_2 at approximately 550ºC, and the conversion of $CaBr_2$ back to CaO and HBr at 730ºC. The second recycle step, converting HBr to Br_2 and generating hydrogen, can be done thermally in a solid-gas, fixed bed reactor of iron oxide, which in turn needs to be regenerated [4,5]. The iron reaction beds can be eliminated in a modified Ca-Br cycle by converting HBr directly to Br_2 and H_2 in a single step. This direct conversion can be performed electrochemically [8-9] or in a plasma process [10].

Aqueous-phase electrolysis suffers from (1) low current densities due to liquid-phase mass-transfer limitations and (2) difficult product separation due to dissolution of Br_2 in solution [8]. Gas-phase electrolysis has been attempted in phosphoric-acid [8,9] and molten-salt cells [10] to address these limitations. Although Br_2 dissolution was avoided in these cells, cell performance was poor.

Results

SO_2 Electrolysys: The results of our work are summarized in Figure 1. In the PEM (Nation 115 membrane) electrolyzer, SO_2 oxidation in the gas phase reduced the cell voltage by over 150 mV at 4.0 kA/m^2 compared to SO_2 oxidation in the liquid phase (*i.e.*, Westinghouse data). This improvement was achieved with one tenth the Pt loading. The process started to become mass-transfer limited at 4.0 kA/m^2 due to limitations in transporting water across the membrane above these currents.

Although the results in Figure 1 are far superior to any previous work, the current was limited to 4 kA/m^2 due to the limitations of water transport across the membrane. To improve water transport, the SO_2 electrolysis was performed with a catalyst-coated Nafion 212 membrane from Lynntech. These results are shown in Figure 2. Since the Pt loading is also different (1.5 mg Pt/cm^2), the same commercial electrode but on Nafion 115 is also shown. The thinner membranes enable us to achieve current densities above 1.2 A/cm^2 (12 kA/m^2). For comparison, the same Westinghouse results shown in Figure 1 are shown here.

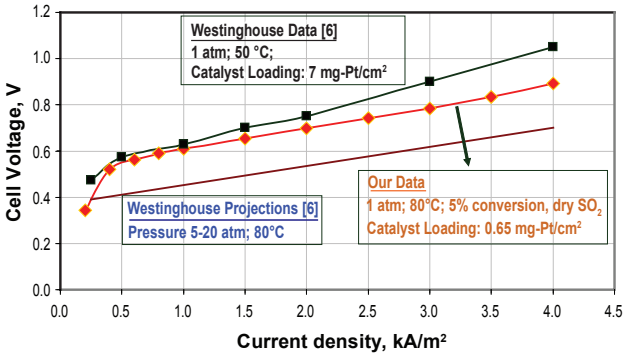

FIGURE 1. The current-voltage response for SO_2 electrolysis in a PEM electrolyzer. Our gas-phase SO_2 results were achieved with a Pt loading one tenth that of Westinghouse's liquid phased process. The membrane was Nafion 115.

HBr Electrolysys: Figure 3 shows the data (♦) for the conversion of HBr to Br_2 and H_2 at 80°C, 1.0 atm and 50% conversion of HBr. The catalyst on both the anode and cathode was 2.0 mg/cm^2 of RuO_2 deposited onto a carbon cloth gas diffusion electrode (ELAT-S® from ETEK). Also shown on this figure are the analogous results for gas and liquid phase HCl electrolysis. This data shows that carrying out halogen chemistry in the gas phase lowers the voltage by approximately 500 mV at 4.0 kA/m^2, which enables the cell to go to higher current densities before carbon corrosion becomes an issue above 2.0 V. Gas phase HBr electrolysis lowers the voltage another 500 mV at that current density. Also shown in Figure 2 is the results from previous gas-phase electrolysis work by Shimizu *et al*. [9]. They ran their cell at 150°C with a Pt loading of 2.5 mg/cm^2. Although their voltages are lower at low current density, a limiting current is observed well before 2.0 kA/m^2 is obtained.

Using the results in Figure 2 as the base case, we investigated the effect of (1) pressure; (2) temperature; (3) percent conversion; and (4) membrane type and thickness.

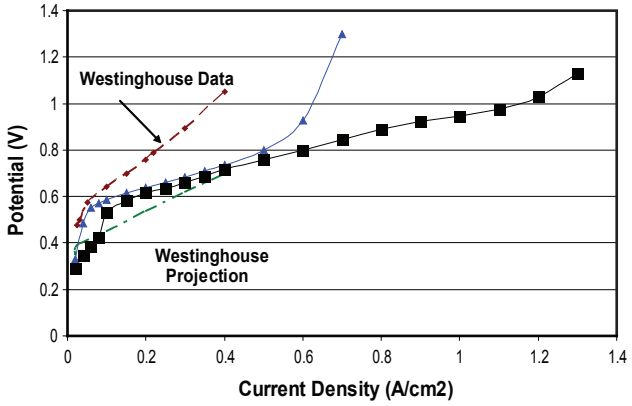

FIGURE 2. The current-voltage response for SO_2 electrolysis in a PEM electrolyzer. The membrane was Nafion 212.

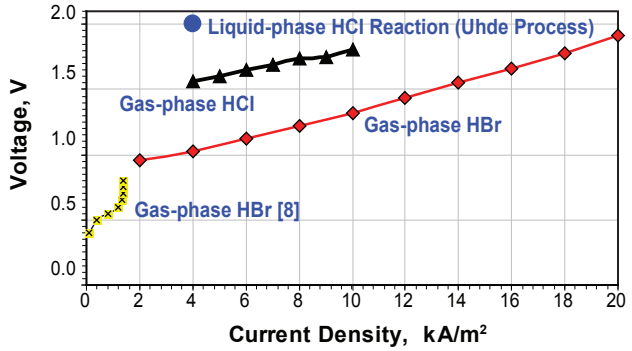

FIGURE 3. The current-voltage response for HBr (♦) electrolysis in a PEM electrolyzer. The HCl data and data from Reference 8 is shown for comparison. The HBr electrolyzer was operated at 80°C, 1.0 atm, and 50% conversion with a RuO_2 loading on the anode and cathode of 2.0 mg/cm^2 and a Nafion 1035 membrane.

Effect of Pressure: We ran the HBr electrolysis in the PEM electrolyzer at 80°C and 50% conversion at pressures of 1.0, 2.0, 3.0, and 4.0 atm. All the data fell on top of the data for 1.0 atm shown in Figure 2. This result was expected since the overall reaction shown in Reaction [3] produces as the same number of moles in the gas phase as it consumes. Therefore, it is expected that H_2 can be produced at any pressure desired without affecting the cell voltage, and hence process efficiency.

Effect of Temperature: We ran the HBr electrolysis in the PEM electrolyzer at 1.0 atm and 50% conversion at temperatures of 60, 70, 80, and 85°C. At 60°C, the curve was shifted up by approximately 100 mV at all currents densities. A run at 100°C and 3.0 atm, which prevented boiling, resulted in a negligible effect on performance over the based case in Figure 2.

Effect of Percent Conversion: As with pressure, percent conversion had no effect on cell voltage. The effect of percent conversion on the water balance will be reported along with the mathematical model in the next report.

Effect of Membrane Type and Thickness: We ran the HBr electrolysis in the PEM electrolyzer at 80°C, 1.0 atm and 50% for three different Nafion membranes, 112, 1035 and 115. The first two numbers in this code indicate average molecular weight of the polymer. The lower number in 1035 means it has a higher density of protons, which increases conductivity. As expected the 115 membrane performed the worst since it was thicker and less conductive that 1035. The 112 membrane gave identical performance to the 1035. The thinner membrane was offset by the higher lower conductivity. Although the voltage was not affected, the water balance was. A detailed report on the humidity of the existing gas stream will be reported along with the mathematical model in the next report.

Mathematical Model of Electrolyzer Performance: A mathematical model of the HBr electrolyzer was developed to predict the current-voltage (I-V) response on the cell and water transport in the system. Due to the Ohmic limitation of the cell evident in the data (see Figure 3), the I-V relationship was fit to the following expression for Ohm's law:

$$V = V^o + IR \qquad [1]$$

where V^0 is the effective open circuit potential and R is the resistance of the membrane-electrode assembly (MEA). Both V^0 and R are functions of temperature and membrane type, but independent of pressure and conversion (i.e., anode flow rate). The resistance R is a weak function of current as evident from the slightly concave shape of the I-V seen in Figure 3.

The water transport in the system is more involved due to the competing effects of diffusion and electro-osmotic drag. The transport model is similar to the modeling work we did for water transport in an HCl electrolyzer [11]. The model will be summarized here, and model predictions will be compared to experimental data obtained from the Nafion 115 membrane.

The diffusional water flux across the membrane decreases in the anode flow direction due to the net transport of water across the membrane into the anode flow channel. The water in the anode flow channel is governed by the following differential equation, which relates the mole fraction of water in the flow direction, z, (y_w) to flux across the membrane ($N_{w,x}$):

$$\frac{N^o_{HBr}}{(1-y_w)^2}\frac{dy_w}{dz} - \left(\frac{w_2}{w_1 d}\right) N_{w,x} = 0 \qquad [2]$$

where w_1 and w_2 are the width of the flow channel and membrane, respectively, and d is the flow channel depth. The inlet molar flux of HBr, N^o_{HBr}, is related to its inlet volumetric flow rate, Q^o_{HBr}, by the idea gas law.

$$N^o_{HBr} = \frac{Q^o_{HBr} P}{RTA} \qquad [3]$$

The flux of water across the membrane is given by:

$$N_{w,x} = -\frac{\rho_M}{M_M \delta \delta_M}\int_{\lambda\lambda_c}^{\lambda\lambda_a} D_{w,F}\, d\lambda\lambda + \frac{\xi\xi\ i}{F} \qquad [4]$$

where the first term on the right hand side is the diffusional flux and the second term is electro-osmotic drag. The water content of the membrane, λ, is defined as the number of moles of water associated with each mole of sulfonic acid side chains in the Nafion membrane. The lower and upper limits of integration seen in the first term are the water content of the membrane at the cathode and anode interfaces, respectively. The water content on the cathode side is constant since it is in contact with pure water. The water content on the anode side varies via Equation [2]. In equation 4, ξ is the electro-osmotic drag parameter and is defined as the number of moles of water transported per mole of protons, from the anode to the cathode. The empirical relationships between $D_{w,F}$ and the mole fraction of water in the anode flow channel were obtained previously [11]. These relationships, along with Equations 2-4, can be used to predict the amount of water in the exiting anode stream (z = L) as a function of current density, flow rate (or % conversion), temperature and pressure. One set of simulations and data are shown in Figure 4 for Nafion 115.

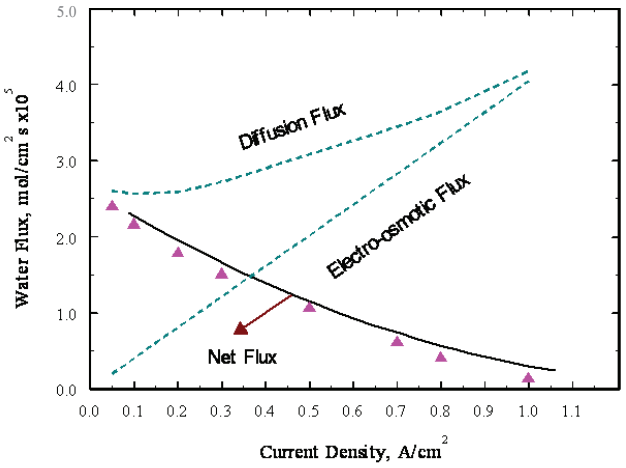

FIGURE 4. Simulations (lines) and experimental data (symbols) of the amount of water in the exiting anode stream (i.e., water flux) as a function of current density. The absolute values of the diffusion and electro-osmotic fluxes are plotted here, with the net flux being the difference between these values. The net flux of water across the membrane is from cathode to anode, and it decreases with an increase in the current density. (membrane = Nafion 115, T = 80°C, P=1.0 atm and Q^0_{HBr} = 870 cc/min [STP]).

Conclusions

A PEM electrolyzer was used for the electrochemical conversion of HBr to Br_2 and H_2, and SO_2 to H_2SO_4 and H_2. The voltage needed to drive this reaction is clearly dominated by the Ohmic resistance (*i.e.*, properties of the membrane). Therefore, it was a weak function of temperature, and independent of pressure and percent conversion. These operating parameters do affect the water balance though. A preliminary mathematical model was developed to predict the water management as a function of design (e.g., membrane type) and operating conditions (e.g., temperature, pressure, current, anode flow rate).

Future Directions

The remaining task is to validate the mathematical model so that it can be fed into overall process models to determine the efficiency, and hence cost, of hydrogen production. The key model predictions that need validating are: (1) current-voltage relationship as a function of temperature; and (2) sulfuric acid concentration as a function of current and temperature. The latter item is the more difficult to simulate and it may require modification to our preliminary water transport model.

References

1. M. A. Rosen, *Int. J. Hydrogen Energy,* **20**, 7, 547 (1995).

2. National Academy of Engineering, "The Hydrogen Economy: Opportunities, Costs, Barriers, and R&D Needs," Chapter 8 (2004).

3. M. A. Rosen, *Int. J. Hydrogen Energy,* **21**, 5, 349 (1996).

4. Nuclear Hydrogen R&D Plan DRAFT; Department Of Energy, Office of Nuclear Energy, Science and Technology, 2004.

5. Nuclear Hydrogen Initiative: Ten Year Program Plan, Office of Advanced Nuclear Research, DOE Office of Nuclear Energy, Science and Technology, March 2005.

6. P. W. Lu, E. R. Garcia and R. L. Ammon, *J. Appl. Electrochem.*, **11**, 347 (1981).

7. P. W. Lu and R. L. Ammon, *J. Electrochem. Soc.,* **127**, 2610 (1980).

8. W. Kondo, S. Mizuta, Y. Oosawa, T. Kumagai, and K. Fujii, "Decomposition of Hydrogen Bromide or Iodide by Gas Phase Electrolysis"; *Bull. Chem. Soc. Jpn.*, **56**, p. 2504 (1983).

9. Y. Shimizu, N. Miura and N. Yamazoe, *Int. J. Hydrogen Energy*, **13(6)**, 345 (1988).

10. C. N. Wauters, and J. Winnick, *AIChE Journal*, **44**(10), 2144-2148 (1998).

11. S. Motupally, A. J. Becker and J. W. Weidner, *J. of the Electrochem. Soc.*, **149**, D63-D71 (2002).

FY 2006 Publications and Presentations

1. P. Sivasubramanian, R. P. Ramasamy, F. J. Freire, C. E. Holland and J. W. Weidner, "Electrochemical Hydrogen Production from Thermochemical Cycles using a Proton Exchange Membrane Electrolyzer," *Int. J. Hydr. Engery*, in press (2006).

2. J. W. Weidner, J. Staser, and P. Sivasubramanian, "Electrochemical Generation of Hydrogen via Thermochemical Cycles," The 1st International Korea-USA Joint Symposium on Hydrogen and Fuel Cells, Daejeon, Korea, May 2006.

3. M. B. Gorensek, W. A. Summers, and J.W. Weidner, "Hybrid Sulfur Cycle Flowsheets for Hydrogen Production from Nuclear Energy," The American Institute of Chemical Engineers Spring Meeting, Orlando, FL, April 2006.

4. J. W. Weidner, P. Sivasubramanian, C.E. Holland and F. Freire, "Electrochemical Generation of Hydrogen via Gas-Phase Oxidation of Sulfur Dioxide and Hydrogen Bromide," The American Institute of Chemical Engineers, Cincinnati, OH, November 2005.

5. J. W. Weidner, P. Sivasubramanian, and R. Ramasamy, "Low Temperature Electrolytic Hydrogen Production in a PEM Electrolyzer," The Electrochemical Society, Los Angeles, CA, October 2005.

Objective #2 -Development of Complex Metal Hydride Hydrogen Storage Materials (Dr. James Ritter)

A series of studies were carried out with $NaAlH_4$ and $LiAlH_4$ doped and processed in novel ways. Highlights from this work over the past year include the following: a synergistic effect of co-dopants on the dehydrogenation kinetics of sodium aluminum hydride was discovered. The effect of graphite on the dehydrogenation and hydrogenation kinetics of Ti-doped sodium aluminum hydride was revealed. A sonochemical doping technique for Ti-catalyzed sodium aluminum hydride was developed. The kinetic behavior of Ti-doped sodium aluminum hydride when co-catalyzed with carbon nanostructures was studied in detail. A physiochemical pathway for cyclic dehydrogenation and rehydrogenation of $LiAlH_4$ was developed. A brief summary of the findings from each of these studies is provided below, along with a graphic or two showing some of the key results.

Synergistic Effects of Co-Dopants on the Dehydrogenation Kinetics of Sodium Aluminum Hydride

A systematic analysis of the effect of co-dopants on the dehydrogenation kinetics of freshly doped and ball milled $NaAlH_4$ samples was carried out with chlorides of Ti, Zr and Fe as the catalysts. Numerous samples of $NaAlH_4$ when co-doped with binary and ternary combinations of Ti, Zr and Fe at 4 mol% total catalyst content exhibited synergistic behavior, with respect to improving the dehydrogenation kinetics of the first decomposition reaction (i.e., $NaAlH_4 \rightarrow Na_3AlH_6$) over that of a sample of $NaAlH_4$ doped with 4 mol% Ti or Zr as single catalysts. In general, the dehydrogenation kinetics improved with the amount of Ti present in a co-doped sample, whether it was a binary or ternary system, with the top five performers all having at least 2 mol% Ti as one of the co-dopants. The binary combination of 3 mol% Ti-1 mol% Fe exhibited the best synergistic performance, with dehydrogenation rates 3.7, 2.0 and 1.5 times that of 4 mol% Ti alone at 90, 110 and 130°C, respectively. The binary co-doped Zr-Fe systems exhibited more pronounced synergistic effects than did the binary co-doped Ti-Fe systems; however, their performance was always worse because Ti is a better single catalyst than Zr. The least synergism was exhibited by the binary co-doped Ti-Zr systems, where it was surmised that the superior electron sharing ability of electron-rich Fe was responsible for it being a better promoter of Ti and Zr than Zr was of Ti. This supposition was further supported by the systematic trends observed with the ternary co-doped systems,

with their synergistic effects seemingly limited to binary combinations of the Ti-Fe and Zr-Fe systems. The effects of Ti, Zr and Fe as co-dopants on the second decomposition reaction (i.e., $Na_3AlH_6 \rightarrow NaH$) were not as pronounced as their effects on the first reaction; but synergisms were still observed, especially with all three binary Zr-Fe co-doped systems and to a lesser extent only with the 3 mol% Ti-1 mol% Fe system. A future study will consider the effects of these co-dopants on the dehydrogenation/rehydrogenation kinetics after cycling. A typical result is shown in Figure 1.

Effect of Graphite on the Dehydrogenation and Hydrogenation Kinetics of Ti-Doped Sodium Aluminum Hydride

The synergistic effect of graphite as a co-dopant on the dehydrogenation and hydrogenation kinetics of Ti-doped $NaAlH_4$ has been observed for the first time. According to temperature programmed desorption curves obtained at 2°C/min, the dehydrogenation temperature in the 90 to 150 °C range decreased by as much as 15°C for $NaAlH_4$ co-doped with 10 wt% graphite (G) and up to 4 mol% $TiCl_3$ compared to similarly doped and ball milled samples without graphite. Constant temperature desorption curves at 90 and 110 °C obtained for $NaAlH_4$ co-doped with 2 mol% $TiCl_3$ and 10 wt% G also, respectively, revealed improvements in the dehydrogenation kinetics of 6.5 and 3.0 times that of a similarly prepared sample without graphite. In contrast, graphite as a single dopant was essentially inactive as a catalyst. The effects of graphite persisted through dehydrogenation/hydrogenation cycling, and through the addition of aluminum (Al) powder, which was added to mitigate irreversible kinetic and capacity losses during cycling. A sample of $NaAlH_4$ co-doped with 2.0 mol% $TiCl_3$, 10 wt% G and 5 wt% Al exhibited perhaps the best dehydrogenation and hydrogenation rates to date. The observed phenomena were interpreted in terms of some of the unique properties of graphite: graphite might be playing a dual role by serving as a mixing agent manifested through lubrication phenomena (i.e., graphene layer slippage and breakage), and as a micro-grinding agent manifested through the formation of carbide species, both during high energy ball milling. In these capacities, graphite may have caused the Ti particles to be more finely ground and hence more dispersed over the surfaces of the $NaAlH_4$ particles and also the graphite particles themselves. Graphite might also be imparting an electronic contribution through the interaction of its facile π-electrons with Ti through a hydrogen spillover mechanism, whereby it back donates some electrons to Ti, which further facilitates hydrogen bond formation and cleavage through this Ti species. Research is continuing with graphite as a co-dopant. Typical results are shown in Figures 2 and 3.

Sonochemical Doping of Ti-Catalyzed Sodium Aluminum Hydride

A new and very effective sonochemical technique has been developed for doping $NaAlH_4$ with metal catalyst prior to high energy ball milling. When $NaAlH_4$ was sonochemically doped with 2 mol% $TiCl_3$ in a decalin slurry using tetrahydrofuran (THF) as a co-solvent and then ball milled, the dehydrogenation temperature in the 90 to 150°C range decreased by about 30°C during temperature programmed desorption (5°C/min) compared to a conventionally wet doped and ball milled sample. Similarly, during constant temperature desorption the dehydrogenation kinetics of sonochemically doped and ball milled samples of $NaAlH_4$ increased by factors of 9.0, 5.1 and 3.1 respectively at 90, 110 and 130°C over those exhibited

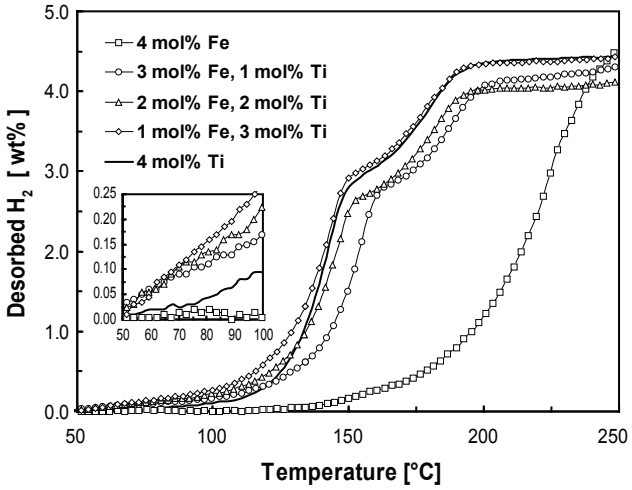

FIGURE 1. Temperature programmed desorption curves at 5°C min^{-1} for $NaAlH_4$ samples just doped and ball milled with 4 mol% catalyst consisting of single and binary combinations of Ti-Fe.

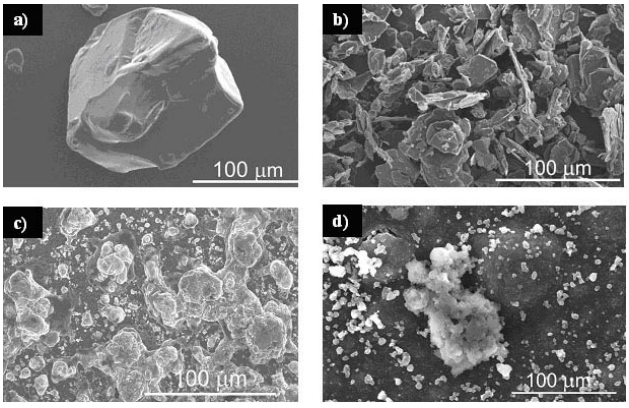

FIGURE 2. Scanning electron microscope images of a) virgin $NaAlH_4$ recrystallized from tetrahydrofuran (THF), b) virgin graphite as received, c) a sample of $NaAlH_4$ doped with 2 mol% Ti (ball milled 2 hrs), and d) a sample of $NaAlH_4$ doped with 2 mol% Ti (ball milled 2 hrs) and 10 wt% G (ball milled an additional 1 hr).

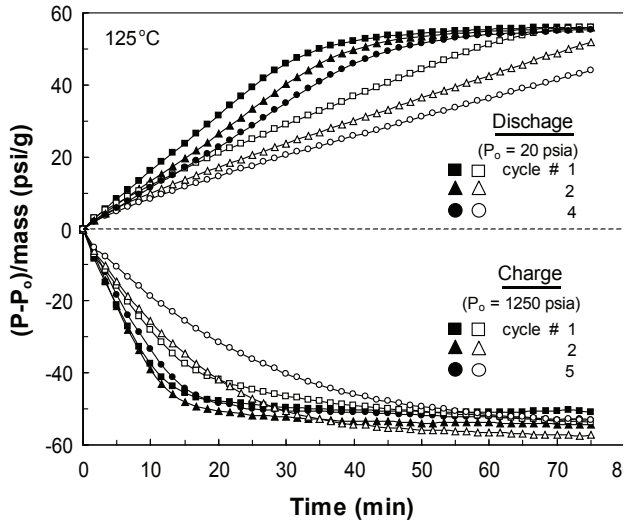

Figure 3. Qualitative hydrogenation and dehydrogenation rates during five charge (P_o = 1,250 psia) and four discharge (P_o = 20 psia) cycles carried out at 125°C for doped and ball milled samples of $NaAlH_4$ containing 2.0 mol% Ti and 5 wt% Al, and 2 mol% Ti, 10 wt% graphite and 5 wt% Al. The filled symbols correspond to samples containing graphite; the empty symbols correspond to samples not containing graphite.

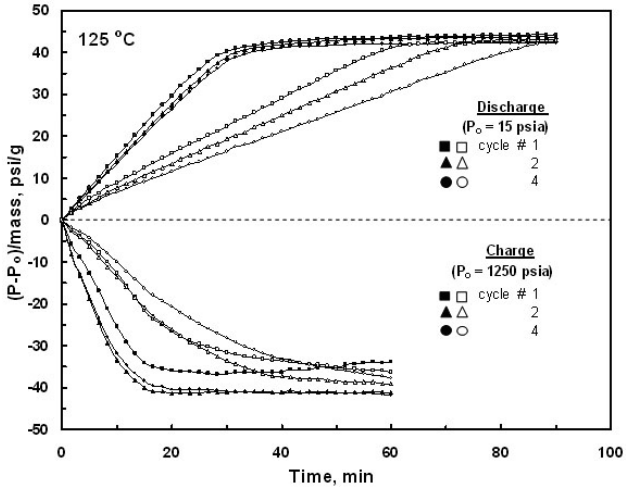

FIGURE 4. Qualitative hydrogenation and dehydrogenation rates obtained during four charge (P_o = 1,250 psia) and four discharge (P_o = 15 psia) cycles carried out at 125°C for ball milled samples of $NaAlH_4$ wet doped and sonochemically doped in decalin with tetrahydrofuran (THF), all doped with 2 mol% Ti. The filled symbols correspond to the sonochemically doped sample; the empty symbols correspond to the wet doped sample.

by conventionally wet doped and ball milled samples. These marked kinetic enhancements persisted through several dehydrogenation/hydrogenation cycles, now with corresponding increases of 16.1, 4.5 and 3.5, and with a striking factor of four improvement in the hydrogenation kinetics also realized at 1,250 psia and 125°C. The observed kinetic effect was interpreted in terms of the complementary mechanochemical effects imparted to the sample by high-intensity ultrasound followed by high energy ball milling. It was surmised that sonochemical doping induced superior mixing of the titanium(III) chloride and sodium aluminum hydride reagents, thereby fostering the formation of smaller catalyst and $NaAlH_4$ particles. This ensured a finer dispersion of the catalyst particles over the surfaces of the $NaAlH_4$ crystals prior to and during the subsequent high energy ball milling process, which greatly improved the mechanochemical effectiveness of ball milling. Strong evidence in support of this supposition stemmed from sonochemical doping being only marginally more effective than conventional wet doping without subsequent ball milling, and scanning electron microscopy images revealing the formation of the factor of ten smaller $NaAlH_4$ particles for the sonochemically doped and ball milled samples. Typical results are shown in Figure 4.

Kinetic Behavior of Ti-Doped Sodium Aluminum Hydride when Co-Catalyzed with Carbon Nanostructures

The effects of single wall carbon nanotubes (SWNTs), multi-wall carbon nanotubes (MWNTs), activated carbon (AC), C_{60} and graphite (G) when used as a co-catalyst with Ti on the dehydrogenation and hydrogenation kinetics of $NaAlH_4$ were investigated for the first time in the important temperature range of 90 to 250°C. All five carbons exhibited significant, sustaining and synergistic co-catalytic effects on the dehydrogenation and hydrogenation kinetics of Ti-doped $NaAlH_4$ that persisted through charge and discharge cycling. SWNTs were the best co-catalyst, G was the worst co-catalyst, and all five carbons were inactive as a catalyst unless Ti was present. The carbon most likely was imparting an electronic contribution through the interaction of its facile π-electrons with Ti through a hydrogen spillover mechanism, which explained why one carbon was better than another one in terms of optimal aromatic character, out-of-plane exposure of π-electrons, and interaction of π-bonds with neighboring sheets. Typical results are shown in Figure 5.

Physiochemical Pathway for Cyclic Dehydrogenation and Rehydrogenation of $LiAlH_4$

A five-step physiochemical pathway for the cyclic dehydrogenation and rehydrogenation of $LiAlH_4$ from Li_3AlH_6, LiH and Al was developed. The $LiAlH_4$ produced by this physiochemical route exhibited excellent dehydrogenation kinetics in the 80–100°C range, providing about 4 wt% hydrogen. The decomposed $LiAlH_4$ was also fully rehydrogenated through the physiochemical pathway using tetrahydrofuran (THF). The enthalpy change associated with the formation of a $LiAlH_4$•4THF adduct in THF played the essential role in fostering

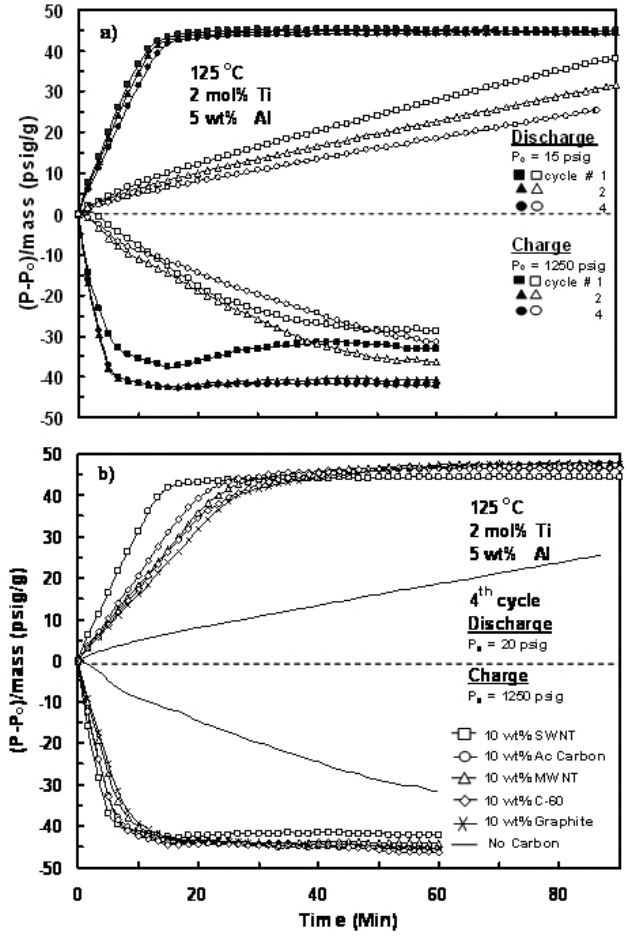

FIGURE 5. Constant temperature cycling curves showing qualitative hydrogenation and dehydrogenation rates: a) during five charge (P_o = 1,250 psig) and four discharge (P_o = 15 psig) cycles at 125°C for doped and ball milled samples of $NaAlH_4$ containing 2.0 mol% Ti and 5 wt% Al, and 2 mol% Ti, 5 wt% Al and 10 wt% SWNT. The filled symbols correspond to samples containing carbon; the empty symbols correspond to samples not containing carbon. b) CTC curves after the 4th charge and discharge cycle for doped and ball milled samples of $NaAlH_4$ containing 2.0 mol% Ti and 5 wt% Al, and 2 mol% Ti, 5 wt% Al and 10 wt% carbon (SWNT, AC, MWNT, C_{60} or G).

this rehydrogenation from the Li_3AlH_6, LiH and Al dehydrogenation products. The kinetics of rehydrogenation was also significantly improved by adding Ti as a catalyst and by mechanochemical treatment, with the decomposition products readily converting into $LiAlH_4$ at ambient temperature and pressures of 3–60 bar. The physiochemical pathway is illustrated in Figure 6 and typical results are shown in Figure 7.

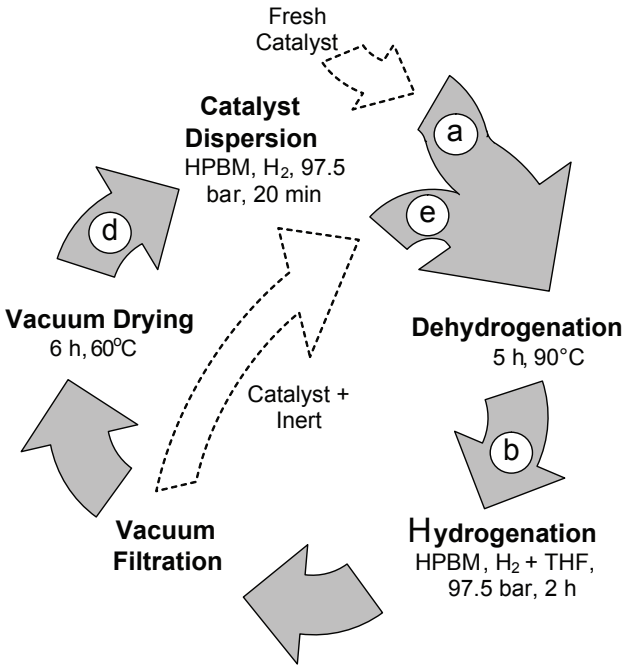

FIGURE 6. Schematic representation of the five-step physiochemical pathway for the cyclic dehydrogenation and rehydrogenation of $LiAlH_4$. The cycle steps consist of catalyst dispersion, dehydrogenation, rehydrogenation, vacuum filtration, and vacuum drying. The conditions listed are not exclusive and correspond to the typical results presented in Figure 2 that were obtained for one complete cycle. The letters in the arrows correspond to the curves in Figure 7.

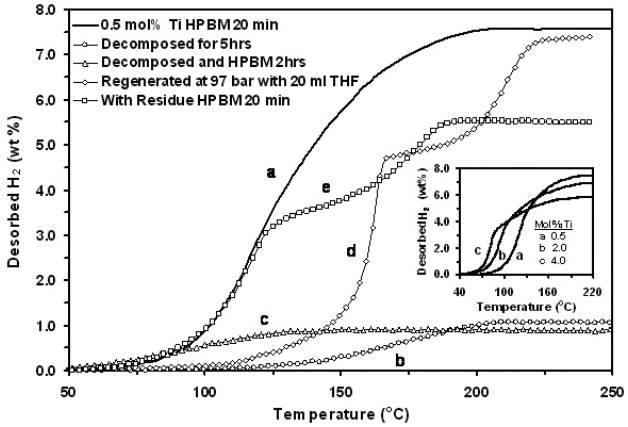

FIGURE 7. Temperature programmed desorption curves (5°C/min) of 0.5 mol% Ti-doped $LiAlH_4$ obtained during one dehydrogenation/rehydrogenation cycle: a) after high pressure ball milling (HPBM) in H_2 at 97.5 bar for 20 minutes to disperse the Ti catalyst; b) after dehydrogenation at 90°C for 5 hours to mimic use of the material in an application; c) after HPBM in H_2 at 97.5 bar for 2 hours after dehydrogenation in a futile attempt to rehydrogenate the sample under dry conditions; d) after HPBM in H_2 at 97.5 bar and 20 ml THF for 2 hours to rehydrogenation the sample under wet conditions, followed by filtration and drying, all being key steps in the physiochemical pathway; and (e) after HPBM in H_2 at 97.5 bar after the residue, obtained from the filtration step and which contains the Ti catalyst and un-converted reactants, was added back to the sample to complete the five-step cycle.

Conclusions and Future Directions

- The series of studies carried out with $NaAlH_4$ and $LiAlH_4$ revealed some novel dopants, combinations of dopants, and processing techniques that not only improved the dehydrogenation and rehydrogenation kinetics of $NaAlH_4$, but that also fostered the reversibility of $LiAlH_4$ under very reasonable conditions through the so-called physiochemical pathway. For example, a synergistic effect of co-dopants on the dehydrogenation kinetics of sodium aluminum hydride was discovered. The effect of graphite on the dehydrogenation and hydrogenation kinetics of Ti-doped sodium aluminum hydride was revealed. A sonochemical doping technique for Ti-catalyzed sodium aluminum hydride was developed. The kinetic behavior of Ti-doped sodium aluminum hydride when co-catalyzed with carbon nanostructures was studied in detail. Finally, a physiochemical pathway for cyclic dehydrogenation and rehydrogenation of $LiAlH_4$ was developed based on the physiochemical pathway.
- Research on the physiochemical pathway is continuing with $LiAlH_4$ and other alanates and boronates. In particular, $LiBH_4$ and $Mg(BH_4)_2$ alone and with combinations of certain alanates and a variety of dopants and processing techniques are being studied. The goal is to develop a reversible hydrogen storage material with very high wt% hydrogen, on the order of 8 to 13 wt%. Although the new materials being explored appear to be reversible only at high temperatures of around 300°C, they could be used with internal combustion engine technology.

Referred Journal Articles

1. J. Wang, A. D. Ebner, R. Zidan, and J. A. Ritter, "Synergistic Effects of Co-Dopants on the Dehydrogenation Kinetics of Sodium Aluminum Hydride," *J. Alloys and Compounds*, **391**, 245-255 (2005).

2. J. Wang, A. D. Ebner, T. Prozorov, R. Zidan, and J. A. Ritter, "Effect of Graphite on the Dehydrogenation and Hydrogenation Kinetics of Ti-Doped Sodium Aluminum Hydride," *J. Alloys and Compounds*, 395, 252-262 (2005).

3. T. Prozorov, J. Wang, A. D. Ebner and J. A. Ritter, "Sonochemical Doping of Ti-Catalyzed Sodium Aluminum Hydride," *J. Alloys and Compounds*, 419, 162-171 (2006).

4. J. Wang, A. D. Ebner, and J. A. Ritter, "Kinetic Behavior of Ti-Doped Sodium Aluminum Hydride when Co-Catalyzed with Carbon Nanostructures," *J. Phys. Chem. B*, 110, 17353-17358 (2006).

5. J. Wang, A. D. Ebner and J. A. Ritter, "Physiochemical Pathway for Cyclic Dehydrogenation and Rehydrogenation of $LiAlH_4$," *J. American Chemical Soc.*, **128**, 5949-5954 (2006).

Patent Applications

1. R. Zidan, J. A. Ritter, A. D. Ebner, J. Wang and C. E. Holland, "Hydrogen Storage Material and Process Using Graphite Additive With Metal Doped Complex Hydrides, Patent Application, US Patent Application 2005/0032641A1 (2005).

2. J. A. Ritter, J. Wang, A. D. Ebner, T. Wang, and C. E. Holland, "Physiochemical Pathway to Reversible Hydrogen Storage," Patent Application, submitted (2006).

Conference Presentations

1. T. Wang, J., Wang, A. D. Ebner, and J. A. Ritter, "Adsorption and Desorption of Hydrogen in Sodium Aluminum Hydride Co-Doped with Zr and Ti," 4th Pacific Basin Conference on Adsorption Science and Technology, Tianjin, China, May 2006.

2. J. Wang, T. Wang, A. D. Ebner and J. A. Ritter, "Physiochemical Pathway to Reversible Hydrogen in Complex Hydrides," TMS 2006: 125th Annual Meeting and Exhibition, San Antonio, TX, March, 2006.

3. J. Wang, T. Prozorov. T. Wang, A. D. Ebner and J. A. Ritter, "Hydrogen Storage in Complex Hydrides: Reversible Reaction that Mimics Adsorption Behavior," AIChE 2005 Annual Meeting, Cincinnati, OH, November 2005.

4. J. A. Ritter, "Is Hydrogen Storage Truly a Roadblock to the Hydrogen Economy?" FuelCellSouth, Columbia, SC May 2005.

Objective #3 – Hydrogen Storage Using Chemical Hydrides (Dr. Michael Matthews)

Introduction

Simple and complex chemical hydrides react with water, either as liquid or vapor, to produce hydrogen. Sodium borohydride has been extensively investigated as a solid hydrogen storage medium. Its reaction with water produces hydrogen and a hydrated solid; the reaction can be written $NaBH_4 + (2+x)\ H_2O \rightarrow 4H_2 + NaBO_2 \cdot xH_2O + \Delta H_r$, where ΔH_r is the heat of reaction. The solid by-product, sodium metaborate can exist in varying degrees of hydration, represented by x, the "excess hydration factor".

Approach

The aim of this project is to develop a hydrogen delivery system based on the gas/solid chemical reaction between steam and chemical hydrides. The use of steam to hydrolyze sodium borohydride overcomes some

disadvantages of the aqueous reaction. Pure steam is contacted with the solid in an enclosed, inert atmosphere reactor at temperatures over 100°C, creating a system with nearly dry reactants and products. This approach can achieve hydrogen yields in excess of 90% of the stoichiometric amount without the need for catalysts or additives. Minimal water is required for this scheme, because the reactants do not need to be dissolved; this improves the mass efficiency of the system.

The primary experimental system is an up-flow packed bed reactor. A mass flow meter is used to measure the hydrogen produced, and the excess water and solid byproducts are collected for analysis. In order to obtain analytical data on water content and crystal structure of the solid byproducts they are analyzed using TGA, DSC, and XRD. ^{11}B-NMR is also used to characterize reaction products and determine overall conversion, leading to a more complete understanding of the reaction pathway.

A group contribution method developed by Li et al. [1] is used to correlate and predict the thermodynamic properties of hydrated borates based on structure and degree of hydration.

Results

Hydrogen yields from 73% to 89% were obtained in the primary packed bed reactor fed with pure steam aqueous solutions of 1 mol% of methanol and 1 mol% of acetic acid were also used. The maximum initial rate of the reaction was about the same regardless of the type of additive, but different yields were obtained. The best yield with methanol (74% to 84%) is no better than yields with pure steam. The use of acetic acid increased yields to 87%-95%. $NaBH_4$ conversion was determined by ^{11}B-NMR analysis of the solid products (see Table 1). For all steam phase reactions, including those with additives, unreacted $NaBH_4$ and $NaBO_2$ were the only boron containing species detected.

A proprietary prototype hydrolysis reactor has been designed to improve practical hydrogen storage capacity. The prototype reactor gave average hydrogen yields of 92% compared to 80% from the primary laboratory reactor. The maximum initial rate of the reaction is also noticeably improved in the prototype system to a measured value of 20.8 mol H_2/min/kg $NaBH_4$. In the primary lab reactor, 50% yield is achieved between 50 to 100 minutes; while in the prototype reactor 50% yield is achieved in less than 10 minutes.

Analysis of solid products and commercial borates confirmed that $NaBO_2 \cdot 2H_2O$ is produced from steam hydrolysis of $NaBH_4$. In some cases the presence of unreacted hydride was also detected in the product. Commercial borate hydrates, $NaBO_2 \cdot 2H_2O$ and $NaBO_2 \cdot 4H_2O$, gradually lose all water when heated through several dehydration steps below 400°C.

Thermochemical calculations show that the steam hydrolysis reactions are strongly favored thermodynamically and very exothermic. The reaction becomes more exothermic with increases in the excess hydration factor, x.

Conclusions and Future Directions

The steam hydrolysis of sodium borohydride can release more than 90% yield of H_2 using only pure water. The reaction rates and yields are slower than what is theoretically expected. The use of methanol did not show any improvement on the rate or yield of the reaction compared to the use of pure steam, while acetic acid promoted the hydrolysis reaction. Analysis of $NaBH_4$ conversions using ^{11}B-NMR was consistent with measured H_2 yields, and indicated that unreacted $NaBH_4$ and $NaBO_2$ are the primary constituents after reaction.

TABLE 1. Primary Reactor Yield and Rate Data

Weight of $NaBH_4$	Reaction Conditions	Max Initial Rate (mol/min/kg)	Measured H_2 Yield	x, Hydration Factor	^{11}B NMR $NaBH_4$ Conversion
0.980 g	Pure Steam	0.843	72.5%	25.7	92.1%
1.179 g	Pure Steam	0.892	85.4%	1.15	90.2%
0.997 g	Pure Steam	0.906	89.1%	3.88	90.0%
1.217 g	1mol% MeOH	0.879	73.7%	2.57	86.8%
1.023 g	1mol% MeOH	0.491	80.6%	12.98	93.3%
1.032 g	1mol% MeOH	0.790	82.8%	10.04	93.3%
1.368 g	1mol% HAc	0.861	87.1%	-	97.5%
1.016 g	1mol% HAc	0.790	91.1%	8.79	95.5%
1.166 g	1mol% HAc	1.044	94.9%	1.87	-

It has been observed that a solution of reactants and products is formed during the steam hydrolysis in both the primary reactor and the prototype. This phase behavior may contribute to the overall mechanism and improved yields. An additional experimental set up is being developed to specifically observe and characterize the formation of a liquid phase solution during reaction at various temperatures and steam saturations. These studies will help determine the reaction pathway and allow for optimization of the phase during reaction.

FY 2006 Publications/Presentations

1. Thomas A. Davis, "Chemical Hydrides for Hydrogen Storage". ***First Annual Korea-USA Joint Symposium on Hydrogen and Fuel Cell Technologies***, Korea. (May 2006)

2. Joshua R. Gray, Eyma Y. Marrero-Alfonso, Thomas A. Davis and Michael A. Matthews. "Steam Hydrolysis of Chemical Hydrides: Meeting the Challenge of Hydrogen Storage". ***Power Sources Conference***, Philadelphia. (June 2006)

3. Eyma Y. Marrero-Alfonso, Joshua R. Gray, Thomas A. Davis and Michael A. Matthews. "Steam Hydrolysis of Chemical Hydrides". ***The Fourth Latin American and Caribbean Conference for Engineering and Technology***, Puerto Rico. (June 2006)

4. Amy M. Beaird, Joshua R. Gray, Eyma Y. Marrero-Alfonso, Michael A. Matthews and Thomas A. Davis. "Characterization of the Gas Phase Hydrolysis of Sodium Borohydride". Submitted to ***AIChE 2006 Annual Meeting,*** San Francisco. (November 2006)

5. Joshua R. Gray, Eyma Y. Marrero-Alfonso, Amy M. Beaird, Casey Campbell, Thomas A. Davis and Michael A. Matthews. "The Application of Steam Hydrolysis of Chemical Hydrides to Facilitate Hydrogen Storage and Generation". Submitted to ***AIChE 2006 Annual Meeting***, San Francisco. (November 2006)

6. Eyma Y. Marrero-Alfonso, Joshua R. Gray, Amy M. Beaird, Thomas A. Davis and Michael A. Matthews. "Reaction Pathways in the Gas/Solid Hydrolysis of Chemical Hydrides as a Novel Approach to Hydrogen Storage and Generation". Submitted to ***AIChE 2006 Annual Meeting,*** San Francisco. (November 2006)

References

1. Li, J.; Li, B.; Gao, S., Calculation of Thermodynamic Properties of Hydrated Borates by Group Contribution Method. Physics and Chemistry of Minerals 2000, 27, (5), 342-346.

Objective #5 – Developing Mathematical Models to Characterize the Performance and Aging of Fuel Cell Cathodes (Dr. Ralph White)

Introduction

Understanding the mechanism of ORR can help to select suitable catalysts and other manufacturing materials of the fuel cell, and optimize operation conditions. Two issues were studied on this objective, one is the double Tafel slope phenomena, and the other is the peroxide presence in the ORR system. Double Tafel slope phenomena were explained by an oxygen adsorption model, and more accurate kinetic parameters can be regressed with this model for ORR than with the normal four electron mechanism. Peroxide is a species highly suspected to cause degradation of the membrane of the fuel cell. It shows up in different degree depend on operation condition and catalyst properties. Rotating ring disc electrode (RRDE) can be used to study the ORR mechanism and monitor the presence of peroxide. Our simulation of polarization curves of ORR on RRDE in 0.5 M H_2SO_4 can greatly help on understanding the characters of RRDE and activities of peroxide in the system.

Approach

The oxygen adsorption model is carefully derived based on prior modeling work in our group. A set of highly nonlinear and tangly coupled partial differential equations subject to a set of complex boundary conditions were solved numerically and iteratively by using FORTRAN language with the facility of a differential equation solver named GNES. Polarization curves are made to study the characters of this model, and a non-linear parameter estimation technique was used to fit the model to experimental data.

The simulation of RRDE is based on a combined model of swirl flow model and Nernst-Planck equations. It is a cylindrical 2-dimensional model with eight partial differential equations. The coding work would be unbearable tedious, but thanks to the commercial software MP, this set of differential equations are solved with reasonable efforts. Polarization curves will be made with a variety of ORR mechanisms to check the possible reaction scheme cause peroxide presence. Two dimensional profiles of concentrations will be shown to characterize the RRDE technique.

Results

The simulated polarization curves made with oxygen adsorption model indicates that this model can predict a transition of Tafel slope. A comparison was made with the normal four electron pathway model by fitting a set of experimental data, and the adsorption model can fit more snugly, as shown in Figure 1. A comparison of polarization curves with the two models using the same kinetic parameters is shown in Figure 2. The inserted Levich-Koutecky plot indicates that the adsorption model can predict the double Tafel slope. The simulation of RRDE is still in process. The MP program is working properly now, and case studies will be done soon.

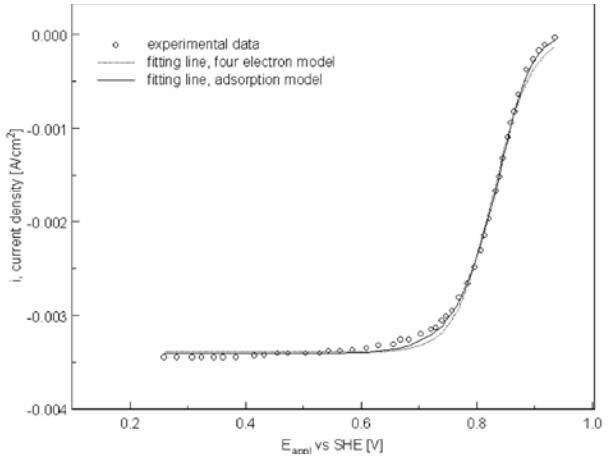

FIGURE 1. Fitting results with experimental data digitized from a figure in the paper by U. A. Paulus et al. [3]. Parameters used to plot: $i_{a,ref}$ = 1e1 A/cm^2 for the adsorption model. See ref [3] for operation conditions.

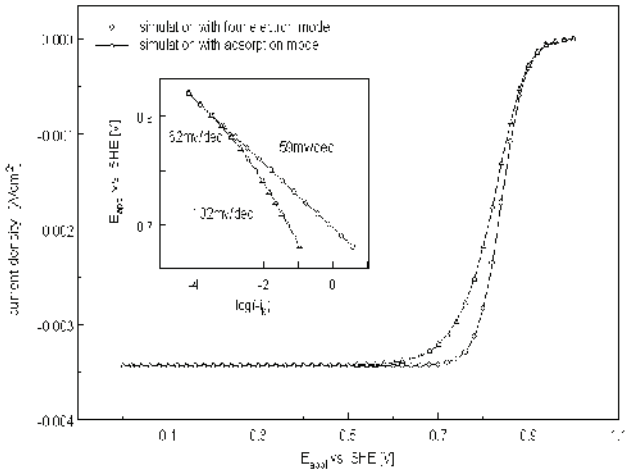

FIGURE 2. Polarization curves simulated with both models. Parameters used to plot: $i_{0,ref}$=1e-8 A/cm^2, α_c =1.0, D_{02}=1.557e-5 cm^2/s for the four electron model, additionally $i_{a,ref}$ = 1e1 A/cm^2 for the model with adsorption term.

Conclusions and Future Directions

Adsorption model can predict the double Tafel slope phenomena, and can fit experimental data better. More accurate parameters maybe extracted with this model for practical use. Simulation of polarization curves on RRDE can be used to characterize the RRDE experiment, and to study the peroxide presence. Our future work will focus on degradation of fuel cells and this simulation will bring us great help.

FY 2006 Publications/Presentations

1. S. Renganathan and R. E. White, "Polymer Electrolyte Membrane Resistance Model," available online at DOE link: http://dx.doi.org/10.1016/j.jpowsour.2006.01.098.

2. Q. Dong, S. Santhanagopalan, R. E. White, "Simulation of the Oxygen Reduction Reaction at a Rotating Disk Electrode in 0.5 M H2SO4 Using an Adsorption Mechanism," submitted to J. Electrochem. Soc.

3. Q. Dong, R. E. White, "Simulation of Polarization Curve of ORR in 0.5 M H_2SO_4 at an RRDE with a Cylindrical 2 D Model Implemented in COMSOL Multiphysics", to be submitted to J. Electrochem. Soc.

References

1. Parthasarathy, C. R. Martin, and S. Srinivasan, J. Electrochem. Soc., **138**, 916 (1991).

2. N. M. Markovic, R. R. Adzic, B. D. Cahan, and E. B. Yeager, J. Electroana. Chem., **377**, 249 (1994).

3. U. A. Paulus, T.J. Schmidt, H. A. Gasteiger, R. J. Behm, J. Electroana. Chem., **495**, 134 (2001).

Objective # 6 – Molecular Simulation of Hydrogen Storage Materials (co-PI Dr. Jerome Delhommelle)

Objectives

The purpose of this new project (starting date: November 1, 2005) is to use molecular modeling to characterize the properties of new hydrogen storage materials (metal-organic frameworks, clathrate hydrates, doped complex hydrides).

Approach

Hydrogen may be stored in solid materials either in a molecular or in an atomic form. The storage of hydrogen in a molecular form takes place in porous materials. The advantage of storing hydrogen in a

molecular form is that molecular hydrogen has fast kinetics. Carbon-based adsorbents, such as carbon nanotubes, were among the first materials investigated [1,2]. While promising, these materials have been beset by mixed results. More recently, metal-organic frameworks (MOFs) [3,4] and clathrate hydrates [5,6] have emerged as systems which could meet the requirements of DOE for automotive fueling. Crystalline MOFs of composition $Zn_4O(BDC)_3$ (BDC=1,4-benzenedicarboxylate) have a cubic three-dimensional extended porous structure. MOFs have been shown to be able to absorb hydrogen at up to 4.5 weight % [4]. Lee et al. [6] have recently shown that clathrates, in which hydrogen molecules are encapsulated or 'occluded' in a cage-like lattice of water molecules, could be used as hydrogen storage at pressures of about 100 bar, i.e. well below the pressure of about 2 kbar reported in previous experiments. This was achieved by adding tetrahydrofuran molecules, which were 'co-occluded' in the clathrate. Lee et al. reported a storage of up to 4% hydrogen by weight under 100 bar. Hydrogen can also be stored in an atomic form. This is typically what happens in complex hydrides [7,8], where hydrogen molecules dissociate on the metal surface.

Results

The mechanism leading to the formation of clathrate hydrates will be investigated using molecular dynamics (MD) simulations. Force fields are already available in the literature for all the compounds considered in this study. More specifically, MD were first performed according to a non-Boltzmann sampling scheme, the so-called umbrella sampling technique. This is because the formation of bulk hydrates is an activated process and is very slow compared with the times accessible by conventional MD methods. These techniques have been used by the co-PI in previous studies of nucleation in supercooled liquids [9].

Conclusions and Future Directions

We are currently investigating the influence of the stabilizer tetrahydrofuran in the formation of clathrate hydrates. This is done using molecular dynamics simulations, together with the non-Boltzmann sampling methods we previously used in our work on nucleation. This is currently under way. The second step consists of extending this study to other type of clathrate hydrates (Lee et al. only looked at a type II structure) and vary the nature of the stabilizer to improve the hydrogen storage capabilities of the binary clathrate. This is also under way.

References

1. L. Sclapbach and A. Zuttel, "Hydrogen-storage Materials for Mobile Applications", *Nature*, 414, 353 (2001).

2. F. Lamari Darkrim, P. Malbrunot and G. P. Tartaglia, "Review of Hydrogen Storage by Adsorption in Carbon Nanotubes", *Int. J. Hydrogen Energy*, 27, 193 (2002).

3. N. L. Rosi, J. Eckert, M. Eddaoudi, D. T. Vodak, J. Kim, M. O'Keefe and O. M. Yaghi, "Hydrogen Storage in Microporous Metal-Organic Frameworks", *Science*, 300, 1127 (2003).

4. L. Pan, M. B. Sander, X. Huang, J. Li, M. Smith, E. Bittner, B. Bockrath and J. K. Johnson, "Microporous Metal Organic Materials: Promising Candidates as Sorbents for Hydrogen Storage", *J. Am. Chem. Soc.* 126, 1308 (2004).

5. W. L. Mao and H. Mao, "Hydrogen Storage in Molecular Compounds", *Proc. Nat. Acad. Sci. USA*, 101, 708 (2004).

6. H. Lee, J.-W. Lee, D. Y. Kim, J. Park, Y.-T. Seo, H. Zeng, H. Zeng, I. L. Moudrakovski, C. I. Ratcliffe and J. A. Ripmeester, "Tuning Clathrate Hydrates for Hydrogen Storage", *Nature*, 434, 743 (2005).

7. B. Bogdanovic and M. Schwickardi, "Ti-doped Alkalimetal Aluminium Hydrides as Potential Novel Reversible Storage Materials", *J. Alloys Comp.* 253, 1 (1997).

8. J. A. Ritter, A.D. Ebner, J. Wang and R. Zidan, "Implementing a Hydrogen Economy", *Materials Today*, September 2003.

9. J.-M. Leyssale, J. Delhommelle and C. Millot, "Reorganization and Growth of Metastable α-N_2 Critical Nuclei into Stable β-N_2 Crystals.", *J. Am. Chem. Soc.* 126, 12286 (2004).